

The Eccentric Frame Decomposition of Central Force Fields

Jared M. Maruskin*, Daniel J. Scheeres[†],
Fred C. Adams[‡] and Anthony M. Bloch[§]

September 15, 2021

Abstract

The rosette-shaped motion of a particle in a central force field is known to be classically solvable by quadratures. We present a new approach of describing and characterizing such motion based on the eccentricity vector of the two body problem. In general, this vector is not an integral of motion. However, the orbital motion, when viewed from the nonuniformly rotating frame defined by the orientation of the eccentricity vector, can be solved analytically and will either be a closed periodic circulation or libration. The motion with respect to inertial space is then given by integrating the argument of periapsis with respect to time. Finally we will apply the decomposition to a modern central potential, the spherical Hernquist-Newton potential, which models dark matter halos of galaxies with central black holes.

1 Introduction

1.1 Central Force Fields

The motion of a particle in a central force field is known to be classically solvable by quadratures. Due to the spherical symmetry of the force field,

*Ph.D. Candidate, Department of Mathematics, The University of Michigan

[†]Associate Professor, Department of Aerospace Engineering, The University of Michigan

[‡]Professor, Department of Physics, The University of Michigan

[§]Professor, Department of Mathematics, The University of Michigan

an angular momentum integral exists and the ensuing motion is confined to a single orbital plane so that, without loss of generality, we can assume the system to have 2 degrees of freedom. In polar coordinates, the Hamiltonian may be expressed as:

$$H = \frac{1}{2} \left(\dot{r}^2 + \frac{h^2}{r^2} \right) - U(r),$$

where $h = r^2\dot{\theta}$ is the angular momentum and $U(r)$ is the potential energy function. We will use the standard convention that dots refer to time derivatives, whereas primes refer to spatial derivatives. The corresponding Hamiltonian system,

$$\dot{r} = v_r \quad \dot{v}_r = \frac{h^2}{r^3} - U'(r) \quad \dot{\theta} = \frac{h}{r^2} \quad \dot{h} = 0,$$

is integrable by quadratures:

$$\int_{r(0)}^{r(t)} \frac{\pm dr}{\sqrt{2H + 2U(r) - h^2/r^2}} = t - t_0 \quad (1)$$

$$\theta(t) = \theta_0 + \int_{t_0}^t \frac{h dt}{r(t)^2}. \quad (2)$$

The ensuing motion follows rosette-shaped paths (Arnold (1989), Whittaker (1988), etc.).

1.2 Osculating Orbital Elements

One could, alternatively, proceed using Variation of Parameters and Lagrange’s Planetary Equations (Brouwer & Clemence (1961), Roy 1988). In this case, one can write down differential equations of motion for the six osculating classical orbital elements and then solve them by quadrature for all time. These equations are nonlinear and furthermore depend upon a choice of the “planetary” gravitational parameter μ . One assumes the potential is a perturbation of a Newtonian potential:

$$U(r) = \frac{\mu}{r} + R(r),$$

where $R(r)$ is known as the *disturbing function*. For a general central force field where there is no nominal attracting body, such a choice is somewhat arbitrary. For instance, there is no primary “planet” when considering motion

in a galactic halo. A gravitational parameter for the unperturbed motion can nonetheless be artificially contrived, perhaps based on the total halo mass (if the motion evolves in the outskirts of the galaxy) or based on the mass of a central galactic bulge or black hole (if the motion evolves near the galactic core). Whatever the choice of gravitational parameter, a complete set of osculating orbital elements arises and the ensuing motion can be determined.

1.3 The Eccentric Frame

We will define a gravitational parameter based on the central force field's potential, with no reference to a main attracting body and perturbation theory. Following the classical analogy, we define $\mu(r)$ such that:

$$U(r) = \frac{\mu(r)}{r}.$$

We will show that this gives rise to a nonstatic eccentricity vector that rotates at a nonuniform rate. The eccentricity vector (Runge-Lenz vector) associated with this spatially variable gravitational parameter function defines a preferred coordinate system which we call the eccentric frame. With respect to this frame, we will show that the motion follows a closed orbit. Depending on the value of energy, the particle will make closed circulations or librations in the eccentric frame. The eccentric frame decomposition gives rise to a set of orbital elements. We will discuss their physical implications and the key features of how they arise. In particular, one can have circular orbits in inertial space with nonzero osculating eccentricity. This feature is not unique to our method, it can arise from any choice of osculating orbital elements. The eccentric frame decomposition, however, illuminates the behavior and gives rise to a new standard description that better fits orbits of central force field potentials.

2 The Eccentric Frame Decomposition

We first define the eccentric frame by means of specifying the nonstatic eccentricity vector associated with the gravitational parameter function $\mu(r) = rU(r)$. We then show that the particle traces a closed orbit as viewed from this noninertial frame. Finally we compute the set of osculating orbital elements that belong to this system.

2.1 Motion with respect to the Eccentric Frame

Given a spherically symmetric potential energy field, we can recast the Hamiltonian into the following form, reminiscent of its classical analogy:

$$E = \frac{1}{2} \left(v^2 + \frac{h^2}{r^2} \right) - \frac{\mu(r)}{r}, \quad (3)$$

where $h = r^2\dot{\theta}$ is the magnitude of the angular momentum vector,

$$\mathbf{H} = \mathbf{r} \times \dot{\mathbf{r}}, \quad (4)$$

and (r, v, θ, h) are the symplectic coordinates, with $v = \dot{r}$. This gives rise to the following Hamiltonian equations of motion:

$$\begin{aligned} \dot{r} &= v & \dot{v} &= \frac{h^2}{r^3} + \frac{\mu'(r)}{r} - \frac{\mu(r)}{r^2} \\ \dot{\theta} &= \frac{h}{r^2} & \dot{h} &= 0 \end{aligned}$$

which can be recast in the following form

$$\ddot{\mathbf{r}} = \left(\ddot{r} - \frac{h^2}{r^3} \right) \mathbf{e}_r = \left(\frac{\mu'(r)}{r} - \frac{\mu(r)}{r^2} \right) \mathbf{e}_r, \quad (5)$$

where $\mathbf{r} = r\mathbf{e}_r$. Consider now the eccentricity vector

$$\mathbf{B} = \dot{\mathbf{r}} \times \mathbf{H} - \mu(r)\mathbf{e}_r. \quad (6)$$

Its evolution is governed by the following equations of motion:

$$\begin{aligned} \dot{\mathbf{B}} &= \dot{\mathbf{r}} \times \mathbf{H} - \mu'(r)\dot{r}\mathbf{e}_r - \mu(r)\dot{\theta}\mathbf{e}_\theta \\ &= \left(\frac{\mu'(r)}{r} - \frac{\mu(r)}{r^2} \right) r^2\dot{\theta}\mathbf{e}_r \times \hat{\mathbf{H}} - \mu'(r)\dot{r}\mathbf{e}_r - \mu(r)\dot{\theta}\mathbf{e}_\theta \\ &= - \left(\frac{\mu'(r)}{r} - \frac{\mu(r)}{r^2} \right) r^2\dot{\theta}\mathbf{e}_\theta - \mu'(r)\dot{r}\mathbf{e}_r - \mu(r)\dot{\theta}\mathbf{e}_\theta \\ &= -\mu'(r)\dot{\mathbf{r}}. \end{aligned}$$

The vector \mathbf{B} itself works out to be

$$\begin{aligned} \mathbf{B} &= r^2\dot{\theta}(\dot{r}\mathbf{e}_r + r\dot{\theta}\mathbf{e}_\theta) \times \hat{\mathbf{H}} - \mu(r)\mathbf{e}_r \\ &= -r^2\dot{r}\dot{\theta}\mathbf{e}_\theta + r^3\dot{\theta}^2\mathbf{e}_r - \mu(r)\mathbf{e}_r \\ &= -h\dot{r}\mathbf{e}_\theta + \left(\frac{h^2}{r} - \mu(r) \right) \mathbf{e}_r. \end{aligned}$$

We thus find the magnitude of \mathbf{B} is:

$$B = \sqrt{2h^2E + \mu^2(r)}. \quad (7)$$

We define the argument of periapsis, ω , to be the angle made between the inertial x -axis and the \mathbf{B} -vector. The \mathbf{B} -vector defines a rotating reference frame, which we call the eccentric frame. We define $\hat{\mathbf{B}}$ to be a unit vector in the \mathbf{B} direction. Hats will denote unit vectors. Let X and Y be the cartesian coordinates of the particle with respect to the eccentric frame and let x and y be the cartesian coordinates of the particle with respect to the inertial frame. The axes of the inertial frame are determined by the stationary unit vectors $\hat{\mathbf{i}}$ and $\hat{\mathbf{j}}$. The polar angle of the particle measured with respect to the $\hat{\mathbf{B}}$ direction is known as the true anomaly f . This notation is also used in Roy (1988). The polar angle of the particle in the inertial frame is related to the true anomaly by the following relation:

$$\theta = f + \omega. \quad (8)$$

In some of the literature, the true anomaly f is denoted by ν ; and the inertial polar angle (argument of latitude) θ is denoted by u . Decomposing the eccentricity vector \mathbf{B} in the inertial frame, we see that

$$\begin{aligned} \mathbf{B} &= \left(\dot{r}h \sin \theta + \left(\frac{h^2}{r} - \mu(r) \right) \cos \theta \right) \hat{\mathbf{i}} \\ &\quad + \left(-\dot{r}h \cos \theta + \left(\frac{h^2}{r} - \mu(r) \right) \sin \theta \right) \hat{\mathbf{j}}. \end{aligned}$$

However, by definition, $\mathbf{B} = B(r)(\cos \omega \hat{\mathbf{i}} + \sin \omega \hat{\mathbf{j}})$. Hence:

$$\begin{aligned} \begin{bmatrix} \cos \omega \\ \sin \omega \end{bmatrix} &= \frac{1}{B(r)} \mathbf{A} \cdot \begin{bmatrix} \cos \theta \\ \sin \theta \end{bmatrix} \\ &= \frac{1}{B(r)} \mathbf{A} \cdot \mathbf{F} \cdot \begin{bmatrix} \cos \omega \\ \sin \omega \end{bmatrix} \end{aligned} \quad (9)$$

where we have defined

$$\mathbf{A} = \begin{bmatrix} (h^2/r - \mu(r)) & \dot{r}h \\ -\dot{r}h & (h^2/r - \mu(r)) \end{bmatrix}$$

and

$$\mathbf{F} = \begin{bmatrix} \cos f & -\sin f \\ \sin f & \cos f \end{bmatrix}$$

and have further made use of the trigonometric identities

$$\begin{aligned}\cos \theta &= \cos(f + \omega) = \cos f \cos \omega - \sin f \sin \omega \\ \sin \theta &= \sin(f + \omega) = \sin f \cos \omega + \cos f \sin \omega.\end{aligned}$$

We recognize that the matrix premultiplying the vector $\langle \cos \omega, \sin \omega \rangle$ on the right hand side of (9) must be the identity matrix. Hence we have found an explicit expression relating the true anomaly and the radius:

$$\cos f = \frac{1}{B(r)} \left(\frac{h^2}{r} - \mu(r) \right) \quad (10)$$

$$\sin f = \frac{1}{B(r)} \dot{r} h. \quad (11)$$

Thus we see that the particle traces out a closed path in the eccentric frame. By carefully considering (11), we see that periapsis is always achieved at $f = 0$, i.e. when \mathbf{r} and \mathbf{B} are parallel; and that apoapsis is achieved at $f = \pi$, i.e. when \mathbf{r} and \mathbf{B} are anti-parallel.

If the angular momentum is positive, (11) tells us that r is increasing when the particle is in the upper half plane and is decreasing when the particle is in the lower half plane. The opposite is true for the case of a negative angular momentum.

2.2 The Osculating Eccentricity and Semi-Major Axis

We would also like to point out that one can rearrange (10) into the following form:

$$r = \frac{h^2/\mu(r)}{1 + B(r) \cos f/\mu(r)} = \frac{p(r)}{1 + e(r) \cos f}, \quad (12)$$

completely analogous to its classical ($\mu(r) = \text{const.}$) form.

Utilizing the relation $p = a(1 - e^2)$, we can define the osculating eccentricity and semi-major axis of the system in closed form as follows:

$$e(r) = \frac{B(r)}{\mu(r)} \quad (13)$$

$$a(r) = \frac{h^2 \mu(r)}{\mu(r)^2 - B(r)^2}. \quad (14)$$

These are given unambiguously as a function of r , without integrating. They represent a standard decomposition of the motion. Using a standard

choice of osculating orbital elements, one would first define a semi-arbitrary choice for a fixed μ . Thus, there is no unique standard set of osculating orbital elements for a general system, rather a one parameter family of orbital elements that describe the motion. By using the radially varying $\mu(r)$, we seek to better normalize the description of motion in such systems.

Since the true anomaly is given by the relations (10) and (11), one now only need solve for the osculating argument of periapsis to obtain the complete motion as a function of time.

2.3 The Osculating Argument of Periapsis

Solving for the osculating argument of periapsis can be done in one of two ways. First, one may integrate (1)-(2) by quadratures. Once r and θ are known, f , a , and e can be extracted by the above relations (10), (11), (13), (14); then the osculating argument of periapsis can be solved by means of the relations $\theta = f + \omega$. On the other hand one can solve the quadrature we derive below.

To determine the rotation of the eccentric frame, consider the angular momentum integral:

$$h = r^2\dot{\theta} = r^2(\dot{f} + \dot{\omega}) = r^2 f'(r) \dot{r} \left(1 + \frac{d\omega}{df} \right). \quad (15)$$

Differentiating (10) and utilizing (11), we have that

$$\begin{aligned} -\sin(f(r))f'(r) &= \frac{-\dot{r}f'(r)h}{B(r)} \\ &= \frac{1}{B(r)} \left(\frac{-h^2}{r^2} - \mu'(r) \right) \\ &\quad - \frac{B'(r)}{B(r)^2} \left(\frac{h^2}{r} - \mu(r) \right). \end{aligned}$$

We can now solve (15) for $\omega'(f)$:

$$\frac{d\omega}{df} = \frac{h}{f'(r)\dot{r}r^2} - 1 = \frac{\Phi(r)}{B(r)h^2 - \Phi(r)} \quad (16)$$

where we define $\Phi(r)$ as:

$$\Phi(r) = \mu(r)r^2B'(r) - B'(r)rh^2 - \mu'(r)r^2B(r). \quad (17)$$

We thus have

$$\omega(f) = \omega(0) + \int_0^f \frac{\Phi(r)}{B(r)h^2 - \Phi(r)} d\tilde{f}. \quad (18)$$

where we recognize $r = r(\tilde{f})$ in the integrand, by the relations (10) and (11). Together with (13) and (14), this constitutes a full set of osculating orbital elements that are well-defined for the orbit for all time.

The full motion is then completely specified in terms of the parameter f by the relation:

$$\theta(f) = f + \omega(f).$$

3 The Zero Velocity Curve

The central force problem is a 2 degree of freedom problem with 2 integrals of motion, E and h . It is therefore integrable and, in fact, reduces to motion on a Liouville torus. The symplectic coordinates of the system are (r, v, θ, h) . The coordinate h is conserved, and the motion therefore takes place on the $h = \text{const.}$ hyper-plane. Motion in the (r, v) plane is constrained to the curve $\Gamma_{h,E}$ defined by (3), with fixed E and h . Meanwhile, θ cycles along S^1 according to $h = r^2\dot{\theta}$. Motion in the reduced (r, v, θ) space can therefore be visualized as follows: it is constrained to the surface obtained by revolving the curve $\Gamma_{h,E}$ around the v axis. This resulting surface is (obviously) topologically equivalent to the Liouville torus, but obtained directly without the arduous task of computing action-angle variables.

For a fixed h , as one varies the energy, one encounters various bifurcation points where the system undergoes changes.

3.1 Periapsis and Apoapsis

Computation of the periapsis and apoapsis radii is accomplished by the standard technique of plotting the zero-velocity curve on the $E - r$ plane. The plot is obtained by setting $v = \dot{r} = 0$ in (3). The resulting equation is:

$$E_{zv}(r) = \frac{1}{2} \frac{h^2}{r^2} - \frac{\mu(r)}{r}. \quad (19)$$

For a fixed energy E , the solutions to this equation represent the periapsis r_p and apoapsis r_a radii. Maximum and minimum values of $E_{zv}(r)$ correspond to unstable and stable circular orbits, respectively. If there are multiple

“wells,” the corresponding roots of this equation alternate $r_{p1}, r_{a1}, r_{p2}, r_{a2}, \dots$, and the forbidden regions of the inertial x-y plane are concentric, circular annuli.

3.2 Circular Orbits

As one decreases the energy for a fixed angular momentum, the curves $\Gamma_{h,E}$ on the (r, v) -plane shrink until they degenerate to a single point on the r -axis which corresponds to a circular orbit in the (r, θ) polar plane. This occurs at the local minima of E on the (r, v) plane, and hence is given by $\nabla E = 0$, where E is given by (3) and h is held fixed. This condition amounts to

$$v = 0 \tag{20}$$

$$\frac{h^2}{r^3} + \frac{\mu'(r)}{r} - \frac{\mu(r)}{r^2} = 0 = \ddot{r}. \tag{21}$$

The root of (21), r_{circ} , corresponds to the radius of the circular orbit which occurs at the minimum energy $E_{\text{circ}} := E_{\text{zv}}(r_{\text{circ}})$.

3.3 Escape Orbits

If $U(r) \rightarrow \text{const.}$ as $r \rightarrow \infty$, a series of unbounded orbits are present in the solution space. Such orbits are classified as escape orbits. Typically one takes the potential at infinity to be zero, so that $U(r) \rightarrow 0$ as $r \rightarrow \infty$, so that orbits with negative energies are gravitationally bounded to the center of the potential, whereas orbits with positive energies have enough energy to escape to infinity.

4 Circulations vs. Librations in the Eccentric Frame

As one decreases the energy from E_{esc} to the minimum energy E_{circ} , one encounters a bifurcation in the eccentric frame at E_{crit} , as the orbits (as seen from the eccentric frame) change from circulations to librations. This is a necessary transition that must occur, as one lowers the energy, before one can reach a circular orbit. It will be our goal in this section to understand the how this bifurcation comes about and to give a qualitative description of motion in the eccentric frame for fixed h as one varies E .

4.1 The Critical Energy

We now define a critical radius and critical energy. The critical radius is defined as the root to the right hand side of (10), which occurs when:

$$h^2 = r\mu(r). \quad (22)$$

For a fixed h , let the solution to (22) be r_{crit} . Further, let us define the critical energy as follows:

$$E_{\text{crit}} = E_{\text{zv}}(r_{\text{crit}}) = -\frac{1}{2} \frac{\mu(r_{\text{crit}})}{r_{\text{crit}}}, \quad (23)$$

where $E_{\text{zv}}(r)$ is given by (19). In the following subsections, we will see how passing through this value of energy brings about a bifurcation in our system.

The critical radius r_{crit} has an important physical significance in terms of the eccentric frame. From (10), we see that $\cos f = 0$, i.e. the particle is crossing the Y -axis in the eccentric frame, exactly when $r = r_{\text{crit}}$. It is interesting to note that r_{crit} is *independent* of the energy of the system. Thus, as one changes the energy, the particle passes between the left and right hand planes through the same two portals ($Y = \pm r_{\text{crit}}$).

As one decreases the energy, the zero velocity curves $r = r_p$ and $r = r_a$ come closer together. Eventually, one will coincide with r_{crit} . This occurs at the critical energy E_{crit} and brings about the bifurcation in the system. For $E < E_{\text{crit}}$, the points $Y = \pm r_{\text{crit}}$ both lie in the forbidden region, thus a transition from the left half to right half plane is no longer possible. If the apoapsis zero-velocity curve $r = r_a$ reaches r_{crit} before the periapsis zero-velocity curve $r = r_p$ does, the particle follows periapsis librations (i.e. librations around periapsis on the right half plane) in the eccentric frame. Alternatively, if the periapsis zero-velocity curve r_p reaches r_{crit} first, the particle follows apoapsis librations.

4.2 The Route to Periapsis Librations

We will first consider the case where it is the apoapsis radius that coincides with r_{crit} at the bifurcation energy E_{crit} . This event brings about periapsis librations for all energies $E < E_{\text{crit}}$. In Fig. 1 and Fig. 2, the path of the particle, for various values of energy, is plotted *with respect to the eccentric frame*, i.e. the X -axis is coincident with the eccentricity vector $\hat{\mathbf{B}}$. As viewed

from this nonuniformly rotating frame, the trajectory of the particle makes closed orbits.

If $E \gg E_{\text{crit}}$, (10) and (11) produce a well-defined closed orbit in the eccentric frame, as seen in Figure 1a.

As E approaches E_{crit} from above, the apoapsis radius slowly approaches the critical radius, and an orbit such as the one seen in Figure 1b is present. Notice the left half of this orbit is nearly circular. This presents some numerical difficulty if one discretizes the radius r and not the true anomaly f . However, this difficulty can be overcome by analytically approximating the left half of the orbit with an ellipse $r_{\text{approx}}(f)$, $f \in [-\pi/2, -\pi] \cup [\pi/2, \pi]$ fitted to the data points $r_{\text{approx}}(\pm\pi/2) = r_{\text{crit}}$ and $r_{\text{approx}}(\pi) = r_a$.

At $E = E_{\text{crit}}$, the apoapsis radius and the critical radius coincide, as shown in Figure 1c. The particle thus reaches the Y -axis of the eccentric frame at the precise moment it reaches the zero velocity curve. Recall that (11) implies that r is increasing in the upper half plane and decreasing in the lower half plane for the case $h > 0$. This bifurcation point is rather interesting, as one only has a half orbit in the eccentric frame. The motion begins at periapsis, but when it reaches the Y -axis, i.e. apoapsis, it ‘‘hops’’ π -radians to the corresponding point on the lower half plane and then returns to periapsis. To compensate there is a corresponding π -radian hop in the argument of periapsis, so that the true polar angle θ is a continuous function of time. This is allowed as the $\frac{d\omega}{df}$ equation, (16), is actually undefined for $\dot{r} = 0$. This is permissible because $B(r_{\text{crit}}) = 0$ exactly if $E = E_{\text{crit}}$, i.e. the eccentricity vector actually vanishes at these endpoints, and then reappears pointing in the opposite direction.

For $E < E_{\text{crit}}$, one sees that $r_a < r_{\text{crit}}$. Thus the portal $X = 0$, $Y = \pm r_{\text{crit}}$ from the right- to the left- half plane lies in the forbidden region. Motion is therefore constrained to the right-half, where periapsis librations arise in the eccentric frame, Figure 1d-1e.

Finally, at $E = E_{\text{circ}}$, the periapsis and apoapsis radii coincide and the trajectory in the eccentric frame degenerates to a single point $X = r_{\text{crit}}$, $Y = 0$, as seen in Figure 1f. The eccentric frame now rotates at a uniform rate and a circular orbit is present in the actual inertial space.

4.3 The Route to Apoapsis Librations

As one sees from Figure 2, the case where the periapsis radius and the critical radius coincide at the bifurcation energy $E = E_{\text{crit}}$ leads to apoapsis librations

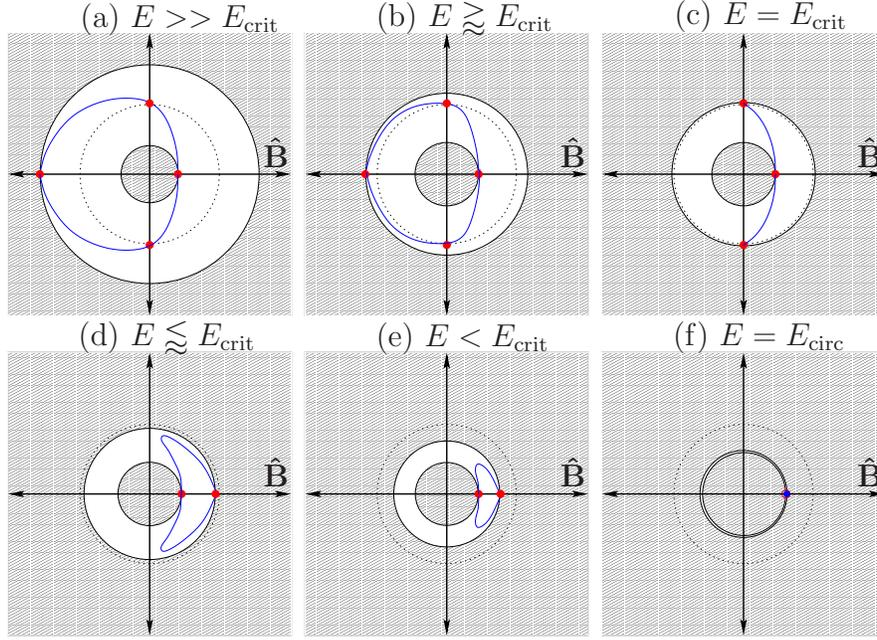


Figure 1: The Route to Periapsis Librations

in the left half plane.

An easy test to determine whether the librations will be periapsis or apoapsis librations is as follows:

$$\begin{aligned}
 r_{\text{circ}} < r_{\text{crit}} &\implies \text{periapsis librations} \\
 r_{\text{circ}} > r_{\text{crit}} &\implies \text{apoapsis librations.}
 \end{aligned}$$

Again one sees that there is a π -radian hop in both true anomaly f and argument of periapsis ω at the bifurcation energy $E = E_{\text{crit}}$. Just before the bifurcation, the right half of the orbit (the half closest to periapsis) is nearly circular.

5 Symmetry of the Rotation

One can exploit the form of the dynamical equation for ω (16) to reduce the numerical integration to one over only one half of an orbit. By examining the differential equation (16), one sees that $\omega'(f)$ depends only upon the radial

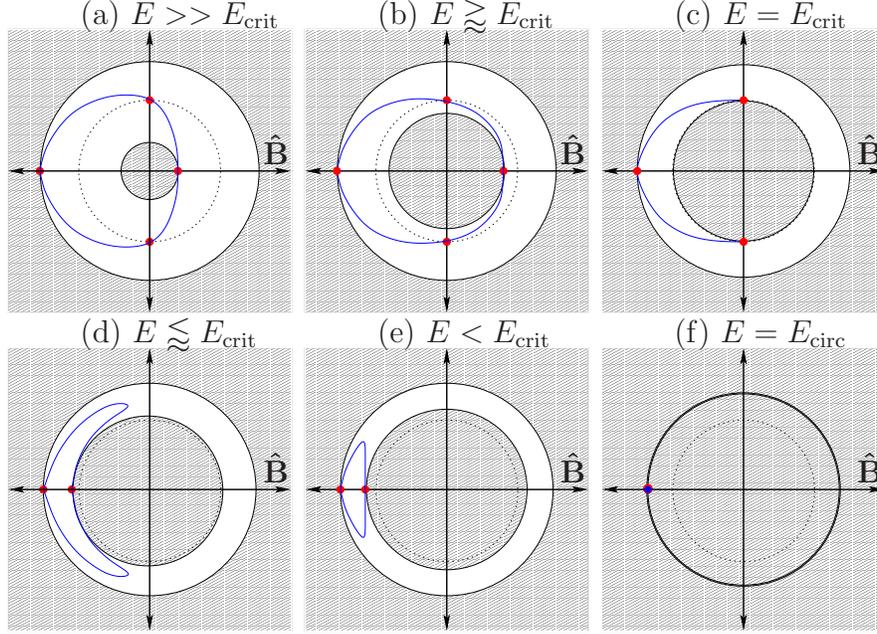


Figure 2: The Route to Apoapsis Librations

coordinate r . Due to the periodicity of the orbit, we have that $\omega'(f)$ is 2π periodic. Moreover, for $f \in [\pi, 2\pi]$, we have that $\omega'(f) = \omega'(2\pi - f)$, since the orbits in the eccentric frame are symmetric with respect to the x -axis.

5.1 Circulations

Prior to the bifurcation ($E > E_{\text{crit}}$) the trajectory makes closed circulations in the eccentric frame. During the circulations, there is a secular growth in the argument of periapsis ω . Define the following:

$$\tilde{\Omega} = \int_0^f \frac{d\omega}{df}(r(\tilde{f})) d\tilde{f} \quad f \in [0, \pi],$$

such that $\tilde{\Omega}$ is the argument of periapsis restricted to the domain $f \in [0, \pi]$. We will show that once one has $\tilde{\Omega}$, one can systematically find $\omega(f)$ for all future f , without integration.

The condition that $\omega'(f) = \omega'(2\pi - f)$ for $f \in [\pi, 2\pi]$ suggests that the function $\omega(f)$ is odd with respect to the axes $f = \pi$ and $\omega = \omega(\pi)$ on

the interval $[0, 2\pi]$. Thus, given $\tilde{\Omega}$ (which we presume has been found by a numerical algorithm), one defines

$$\Omega(f) = \begin{cases} \tilde{\Omega}(f) & f \in [0, \pi] \\ 2\tilde{\Omega}(\pi) - \tilde{\Omega}(2\pi - f) & f \in (\pi, 2\pi] \end{cases} .$$

The net secular growth in $\omega(f)$ over one nominal orbit $0 \leq f \leq 2\pi$ is given by

$$\Delta\Omega = \Omega(2\pi).$$

$\omega(f)$ can subsequently be found by applying the following:

$$\omega(f) = n\Delta\Omega + \Omega(f \bmod 2\pi),$$

where n is the orbit number, i.e. $n = 0$ if $f \in [0, 2\pi]$, $n = 1$ if $f \in [2\pi, 4\pi]$, etc.

6 The Hernquist-Newton Potential

To illustrate the theory in the context of a modern problem, we will consider motion of a particle (star) in a spherical galaxy, modelled with the Hernquist potential, with a central black hole. These results could be similarly applied to a black hole at the center of a globular cluster, or various other astrophysical configurations that yield spherical or azimuthal symmetry. In this context, the central black hole provides a classical point potential, but no general relativistic effects are included.

6.1 Galactic Halos with Central Black Holes

The Hernquist potential has achieved some acclaim in recent years for its ability to analytically model galactic dark matter halos, see Hernquist (1990). We will consider here a coupling between the spherical Hernquist profile and a Newtonian point mass, assumed to model a black hole at the center of the galaxy. Some numerical modelling of triaxial galaxies with central black holes has already been carried out, as in Poon & Merrit (2004).

Let μ_{BH} and μ_{halo} be the gravitational parameters of the central black hole and the galactic dark matter halo, respectively; and let b be a length

scale of the galaxy (so that $M(b) = M_{\text{tot}}/4$, see Hernquist (1990)). Then the Hernquist-Newton potential can be written:

$$U(r) = \frac{\mu_{\text{halo}}}{R+b} + \frac{\mu_{\text{BH}}}{R}.$$

By defining:

$$\mu_0 = \mu_{\text{halo}} + \mu_{\text{BH}} \quad \tilde{\mu} = \frac{\mu_{\text{halo}}}{\mu_{\text{halo}} + \mu_{\text{BH}}},$$

the Hernquist-Newton potential can be recast into the following equivalent form:

$$U(r) = \frac{\mu_0}{R} \left(1 - \frac{\tilde{\mu}}{1 + R/b} \right)$$

with associated Hamiltonian:

$$\mathcal{E} = \frac{1}{2} \left[\left(\frac{dR}{dT} \right)^2 + \frac{H^2}{R^2} \right] - \frac{\mu_0}{R} \left(1 - \frac{\tilde{\mu}}{1 + R/b} \right). \quad (24)$$

where $H = R^2 \frac{d\theta}{dT}$ is the angular momentum. As this is a central force field, the angular momentum and energy will be conserved quantities. Observe that when $\tilde{\mu} = 0$, the potential energy reduces to that of a Newtonian point mass. When $\tilde{\mu} = 1$, the potential energy is equivalent to the Hernquist potential. For $0 < \tilde{\mu} \ll 1$, the model represents a Newtonian point mass with a surrounding ‘‘Hernquist cloud’’ and for $0 \ll \tilde{\mu} < 1$, we have the Hernquist potential with a relatively weak point mass at the origin, which could be used to model a spherical Hernquist galaxy with a central black hole.

6.2 Nondimensionalization

Carrying out the following change of variables:

$$R = rb \quad T = \sqrt{\frac{b^3}{\mu_0}} t,$$

and thus, consequently,

$$H = \sqrt{b\mu_0} h \quad \mathcal{E} = \frac{\mu_0}{b} E,$$

we can recast the Hamiltonian (24) into the following form:

$$E = \frac{1}{2} \left(\dot{r}^2 + \frac{h^2}{r^2} \right) - \frac{\mu(r)}{r}, \quad (25)$$

where we define

$$\mu(r) = \left(1 - \frac{\tilde{\mu}}{1+r} \right). \quad (26)$$

We have thus recast the Hernquist-Newton potential to a one-parameter family of potentials, with $\tilde{\mu} = 1$ corresponding to a the Hernquist potential and $\tilde{\mu} = 0$ corresponding to a pure Newtonian point mass.

We note that the Hernquist-Newton potential is similar to analogous work on the Manev problem, which considers a potential of the form $U(r) = A/r + B/r^2$. In fact, work has been carried out for the anisotropic Manev problem, which replaces the radial coordinate r with an ‘‘elliptic radius’’ $m = \sqrt{\mu x^2 + y^2}$ (e.g., Craig et al. 1999, Diacu & Santoprete 2001). In this type of potential, one obtains a large class of chaotic orbits as well as nonchaotic orbits.

6.3 Zero Velocity Curves

Using the relationship for circular orbits (21) and the critical energy condition (22), sample values of circular radius and energy, critical energy, and the critical periapsis and apoapsis are shown in Table 1, where we have taken $h = 0.1$. The critical radius r_{crit} coincides with the critical energy periapsis radius $r_{\text{crit}}^{\text{peri}}$ in each case, so that the bifurcation always leads to apoapsis librations.

$\tilde{\mu}$	r_{circ}	E_{circ}	E_{crit}	$r_{\text{crit}}^{\text{peri}}$	$r_{\text{crit}}^{\text{apo}}$
1	0.2500	-0.7200	-0.4524	0.1051	1.1932
0.99	0.2274	-0.7539	-0.5000	0.1000	1.000
0.95	0.1508	-0.9372	-0.7440	0.0820	0.4460
0.90	0.0938	-1.3206	-1.1960	0.0647	0.1645

Table 1: Various physical quantities for $h = 1$

The zero-velocity curves are plotted in Fig. 3 below for $h = 0.1$ and for the same values of $\tilde{\mu}$ as in Table 1.

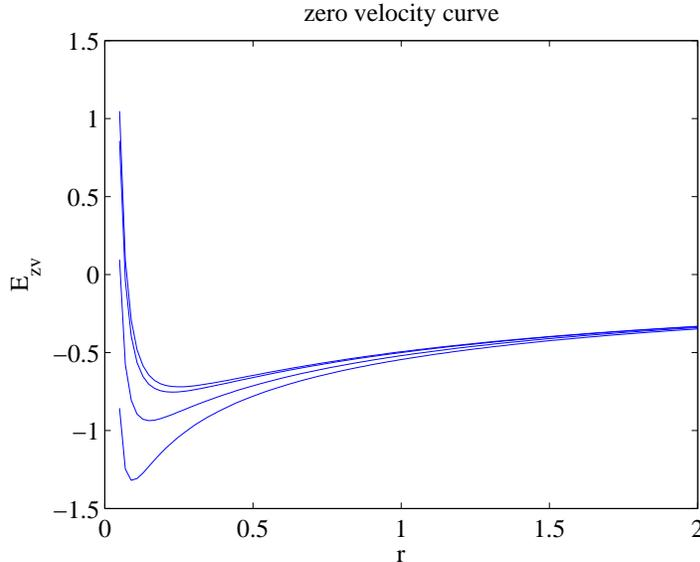


Figure 3: Zero Velocity Curves with $h = 1$ and, from top down, $\tilde{\mu} = 1, 0.99, 0.95, 0.9$

6.4 Orbits for $h = 0.1$

We examine a sample of orbits in the eccentric and inertial frames for various energies at $h = 0.1$. The zero velocity curve for this angular momentum is plotted in Fig. 4 below.

For a sample orbit with $E > E_{\text{crit}}$, we take $E = -0.6$. The orbit as seen from the eccentric and inertial frames is shown in Fig. 5.

Upon integrating (18), one obtains $\omega(f)$, which can be seen for this orbit plotted in Fig. 6. One sees $\Delta\omega = \omega(2\pi) - \omega(0)$ is the *turning angle* of the rosette. For energies prior to (above) the critical bifurcation energy, we find a secular retrograde rotation of the eccentric frame. $\theta(t)$, $\omega(t)$, and $f(t)$ are plotted against time over three standard orbits on the right. One sees a secular prograde growth in the inertial polar angle θ , with turning angle $\Delta\theta = 2\pi + \Delta\omega$. (Recall that $\Delta\omega < 0$).

Finally, we compute the osculating semi-major axis and eccentricity vs. time (Fig. 7) over one nominal orbit (as seen from the eccentric frame). The solid lines represent the osculating elements as provided by the eccentric frame method, see (13)-(14). The dashed curves are a standard set using the

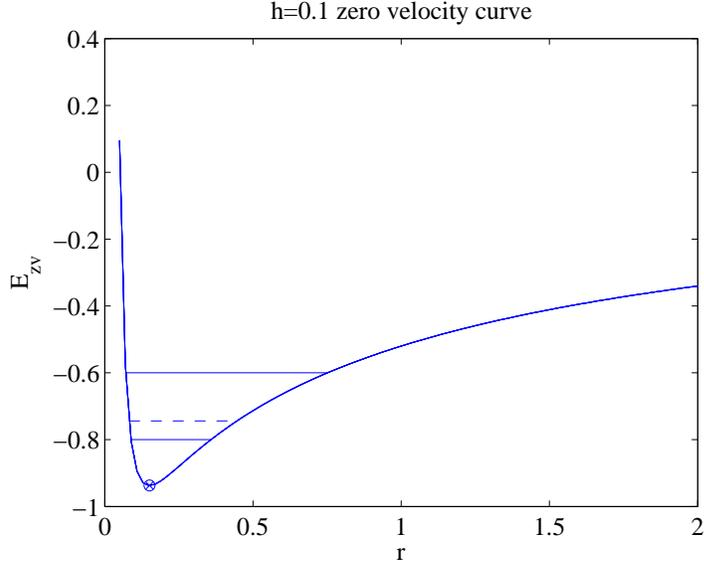


Figure 4: Zero Velocity Curves and sample orbits at $h = 0.1$; $E = -0.6, E_{\text{crit}}, -0.8, E_{\text{circ}}$

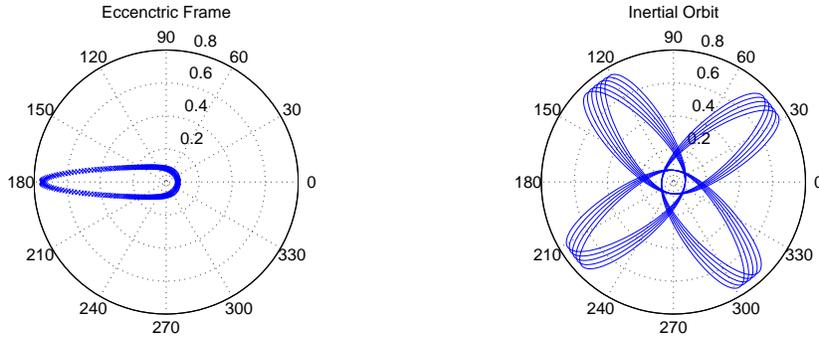


Figure 5: $E = -0.6$ orbit in eccentric (left) and inertial (right) frames

osculating orbital element transformation as defined by classical perturbation theory, using $\mu_0 = 1$ for the “planet” mass, i.e. μ_0 is the gravitational parameter of the *total* halo mass *plus* the mass of the central black hole.

For a sample orbit with $E < E_{\text{crit}}$, we take $E = -0.8$. The orbit as seen

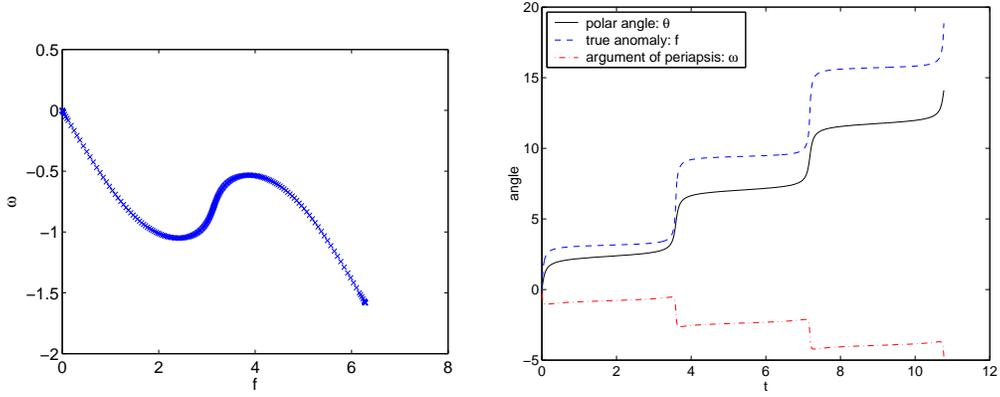


Figure 6: $\omega(f)$ (left) and $\theta(t)$, $\omega(t)$, $f(t)$ (right) for $E = -0.6$

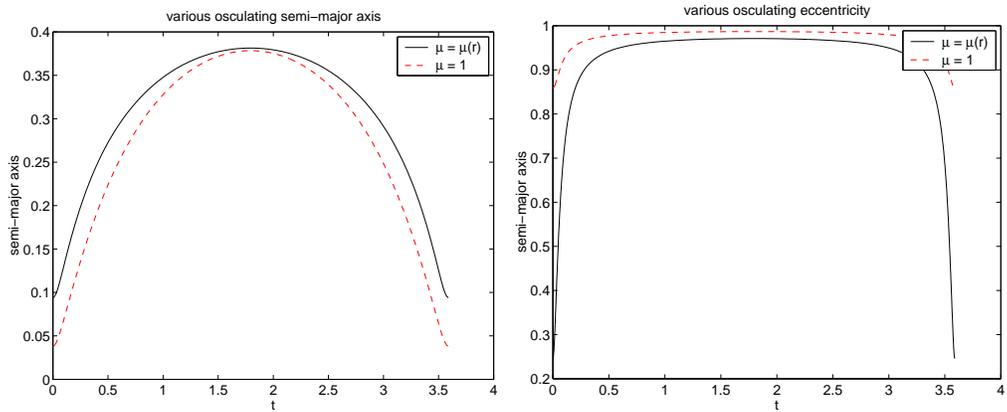


Figure 7: Osculating orbital elements for $E = -0.6$

from the eccentric and inertial frames is shown in Fig. 8. Notice that the particle now makes librations in the eccentric frame. The libration paths become smaller and smaller until they degenerate to a single point at E_{circ} , to be considered next.

$\omega(f)$ for this orbit is plotted in Fig. 9. Notice that f librates around $f = \pi$ and there is secular prograde growth in ω . The turning angle is still given by $\Delta\omega$. For energies after (below) the critical bifurcation energy, we find a secular prograde rotation of the eccentric frame. $\theta(t)$, $\omega(t)$, and $f(t)$

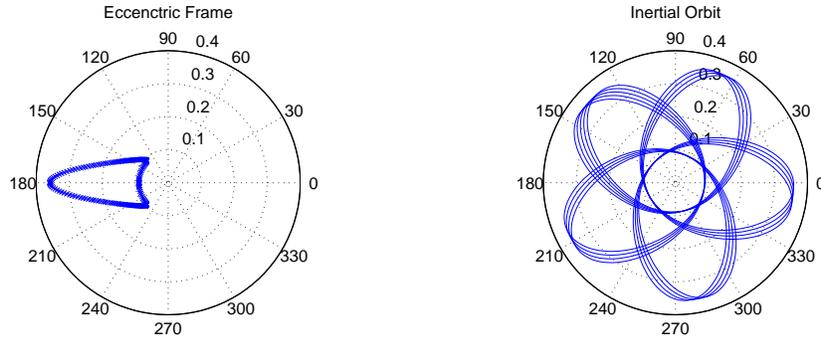


Figure 8: $E = -0.8$ orbit in eccentric (left) and inertial (right) frames

are plotted against time over three standard orbits on the right. One now sees a secular prograde growth in the argument of periapsis, coupled with librations in true anomaly f .

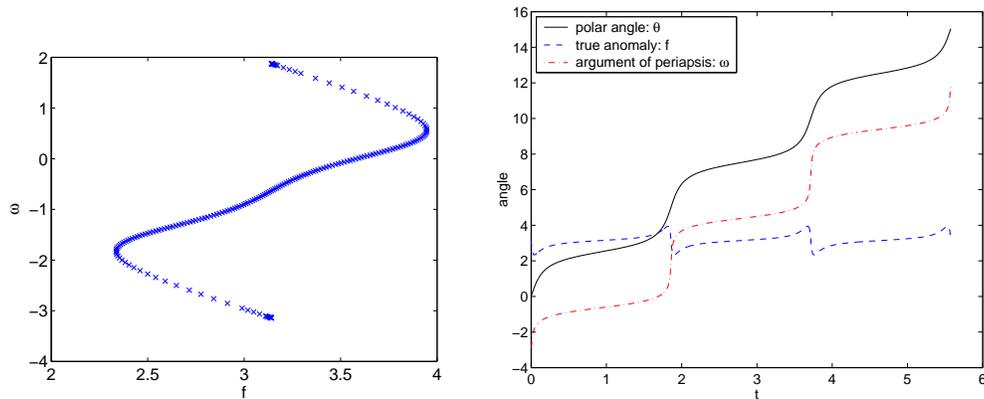


Figure 9: $\omega(f)$ (left) and $\theta(t)$, $\omega(t)$, $f(t)$ (right) for $E = -0.8$

Finally, we compute the osculating semi-major axis and eccentricity vs. time (Fig. 10) over one nominal orbit (as seen from the eccentric frame). The solid lines represent the osculating elements as provided by the eccentric frame method, see (13)-(14). As before, the dashed curves are a standard set using the osculating orbital element transformation as defined by classical perturbation theory, using $\mu_0 = 1$ for the “planet” mass, i.e. μ_0 is the

gravitational parameter of the *total* halo mass *plus* the mass of the central black hole.

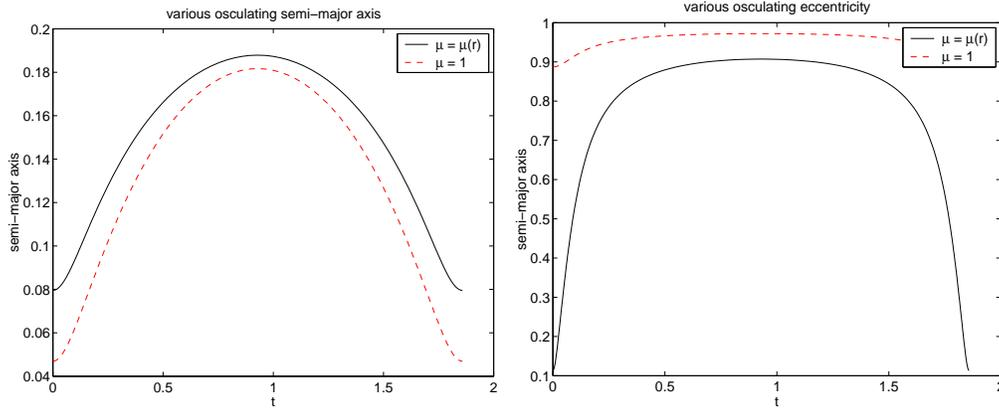


Figure 10: Osculating orbital elements for $E = -0.8$

At the circular energy $E = E_{\text{circ}}$, the orbit in the eccentric frame degenerates to a single point. The orbit is circular in the inertial plane, Fig. 11. The eccentric frame now precesses at a uniform rate.

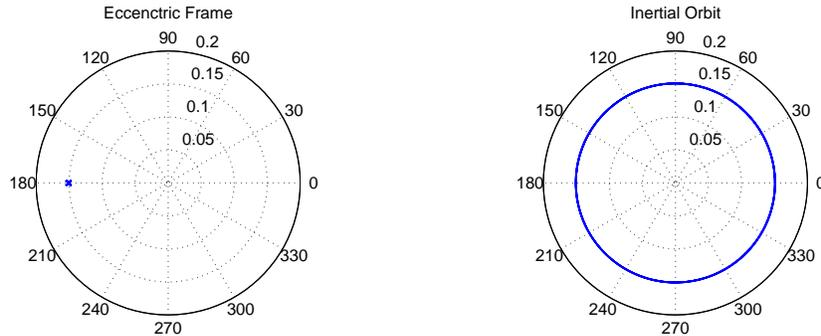


Figure 11: $E = -0.9372$ orbit in eccentric (left) and inertial (right) frames

$\omega(f)$ (left) and $\theta(t), \omega(t), f(t)$ are plotted below in Fig. 12. Now f is virtually constant and there is uniform growth in ω .

Finally, when observing the semi-major axis and eccentricity of the orbit (Fig. 13), we see something counterintuitive. The osculating eccentricity is

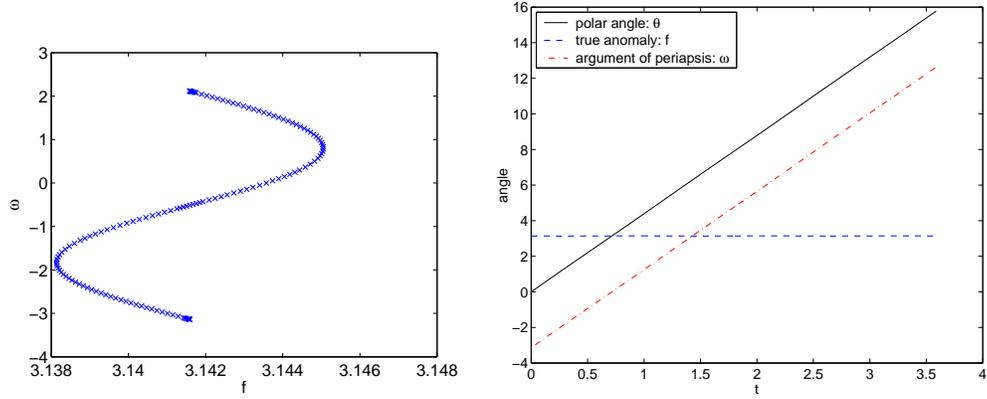


Figure 12: $\omega(f)$ (left) and $\theta(t)$, $\omega(t)$, $f(t)$ (right) for $E = -0.9372$

close to 0.62. If one, on the other hand, used a classical definition of osculating orbital elements, as previously discussed, the osculating eccentricity would be close to 0.94. We thus see a circular orbit (in inertial space) with high osculating eccentricity. The osculating ellipse is a highly eccentric one that always touches the true path at apoapsis. In this way, the osculating ellipse rotates synchronously with the particle so that the particle is always at apoapsis and the true motion is a circular path.

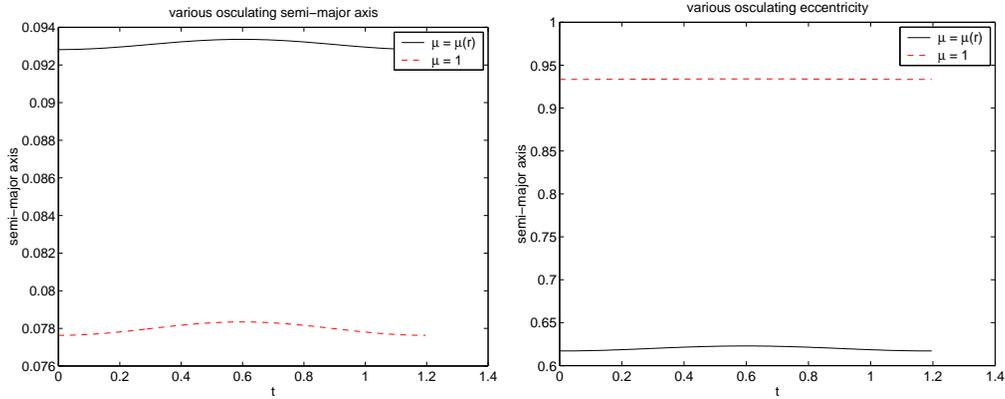


Figure 13: Osculating orbital elements for $E = -0.9372$

7 Stability Analysis of Equatorial Rosettes in Axi-symmetric Potentials

In this section we will consider the stability of the planar equatorial motion of a particle in an axi-symmetric potential. On the plane of symmetry, the potential reduces to a two-dimensional central force field. Since the motion is periodic with respect to the eccentric frame, the technique justifies application of Floquet theory for the stability analysis of the in-plane motion, where the period used is the period of the orbit in the eccentric frame.

7.1 Floquet Theory

Suppose now we are considering a conservative system with axi-symmetric equipotential contours, so that, in cylindrical coordinates, the potential energy is given by $U(r, z)$. We can define a variable gravitational parameter by $\mu(r, z) = rU(r, z)$. The Hamiltonian of the system is thus given by:

$$H = \frac{1}{2} \left(v_r^2 + \frac{h_z^2}{r^2} + v_z^2 \right) - U(r, z)$$

where the symplectic coordinates are $\langle r, v_r, \theta, h_z, z, v_z \rangle$. The equations of motion are:

$$\begin{aligned} \dot{r} &= v_r & \dot{v}_r &= \frac{h_z^2}{r^3} + \frac{\partial U(r, z)}{\partial r} \\ \dot{\theta} &= \frac{h_z}{r^2} & \dot{h}_z &= 0 \\ \dot{z} &= v_z & \dot{v}_z &= \frac{\partial U(r, z)}{\partial z}. \end{aligned}$$

In particular, equatorial motion with $z \equiv 0$ is well defined, and this reduces to the problem of motion in a central force field. The resulting motion follows a rosette-shaped path in the equatorial plane. We now ask whether this motion is stable under a small out-of-plane perturbation δz . To do this, we consider the 2×2 out-of-plane State Transition Matrix (STM) Φ , which, by definition, gives:

$$\begin{bmatrix} \delta z(t) \\ \delta \dot{z}(t) \end{bmatrix} = \Phi \cdot \begin{bmatrix} \delta z(0) \\ \delta \dot{z}(0) \end{bmatrix}.$$

The STM is determined by integrating the following differential equation:

$$\dot{\Phi}(t) = \begin{bmatrix} 0 & 1 \\ U_{zz}(r, 0) & 0 \end{bmatrix} \cdot \Phi(t), \quad \Phi(0) = \begin{bmatrix} 1 & 0 \\ 0 & 1 \end{bmatrix},$$

where the coefficient matrix is evaluated along the nominal orbit ($z = 0$) in the equatorial plane. Since the equatorial motion reduces to a central force field problem, there exists an eccentric frame decomposition, in which the motion is periodic. Let T be the period of a single orbit in the eccentric frame. The coefficient matrix, above, only depends on $r(t)$, and thus it is T -periodic. We are therefore justified in using Floquet theory in the stability analysis. Let λ_1, λ_2 be the eigenvalues of $\Phi(T)$. Since $\lambda_1 \lambda_2 = 1$, either the eigenvalues are complex conjugates on the unit circle in the complex plane, or real-valued with $\lambda_2 = \lambda_1^{-1}$. The rosetal motion on the equatorial plane is therefore stable if and only if both eigenvalues are on the unit circle. A bifurcation from stable to unstable must occur when $\lambda_1 = \lambda_2 = 1$.

7.2 Application to a toy axi-symmetric potential

To show how this theory might be applied, we will consider the following toy potential:

$$U(R) = \frac{1}{R} \left(1 - \frac{1}{1+R} \right) = \frac{\mu(R)}{R}, \quad \text{where } R = \sqrt{r^2 + \frac{z^2}{a^2}}.$$

Here, $r = \sqrt{x^2 + y^2}$ and $a > 0$ is a parameter. When $a < 1$, the potential is oblate spheroidal, and when $a > 1$, it is prolate. This potential is motivated by replacing r with R in (26), but does not have direct physical significance. Its utility to us is only to illustrate the theory. The potential reduces to the Hernquist potential when restricted to the equatorial plane. The question now arises, for various values of the parameter a , when is the equatorial motion due to out of plane perturbations stable? Clearly, for $a = 1$, the motion is stable due to the angular momentum integral. To proceed, we compute the out of plane dynamics:

$$\ddot{z} = \frac{\partial U}{\partial z} = \frac{-\mu(R)}{R^3} \frac{z}{a^3} + \frac{\mu'(R)}{R} \frac{z}{Ra^2}.$$

For a small perturbation δz , we obtain:

$$\delta \ddot{z} = \omega(t) \delta z = \left(\frac{-\mu(r)}{a^2 r^3} + \frac{\mu'(r)}{a^2 r^2} \right) \delta z.$$

The coefficient $\omega(t)$ is a function of time because we have an explicit solution for $r(t)$ for the nominal motion along the equatorial plane. The out of plane State Transition Matrix (STM) for $\langle \delta z, \delta \dot{z} \rangle^T$ can then be written as:

$$\dot{\Phi} = \begin{bmatrix} 0 & 1 \\ \omega(t) & 0 \end{bmatrix} \cdot \Phi, \quad \Phi(0) = \begin{bmatrix} 1 & 0 \\ 0 & 1 \end{bmatrix}.$$

The STM Φ can now be integrated along with the nominal planar solution, as its dynamic coefficient matrix depends only on $r(t)$. We can now systematically integrate $\dot{\Phi}$ between $t \in [0, T]$, where T is the eccentric frame orbital period. Computing the eigenvalues of $\Phi(T)$ reveals the stability of the planar equatorial orbit.

We followed this procedure for a sampling of different energy levels and axis ratios $1 : 1 : a$. The result for oblate potentials is shown in Fig. 14. The grid points with dots correspond to parameter values of a and E for which the equatorial motion is unstable. For prolate potentials, the result is similarly depicted in Fig. 15. Notice in both plots, for $a = 1$, that the planar motion is stable for all energies.

8 Conclusion

In this paper we presented a preferred, nonuniformly rotating frame that exists for motion in any central force field, with respect to which the orbital motion is periodic. We showed that for high values of energy, the particle trajectories in the eccentric frame make circulations. However, when the energy drops beneath a certain critical level, the trajectories follow librations in the eccentric frame. This is not a true bifurcation of the system, as there is no distinguishable physical change when the orbits are viewed with respect to inertial space, yet it is a necessary transition that must occur as one nears the minimum circular orbit energy. For circular orbits (in inertial space), motion in the eccentric frame degenerates from librations to a single fixed point. For this case, the eccentric frame rotates at a constant rate, and a circular orbit in inertial space is observed. Further we showed that, even in the case of a circular orbit, the osculating eccentricity can be very high. This occurs because the particle is “stuck” to the periapsis or apoapsis of the osculating ellipse. The osculating ellipse has static (high) eccentricity and rotates at a uniform rate. We also presented a model for the potential

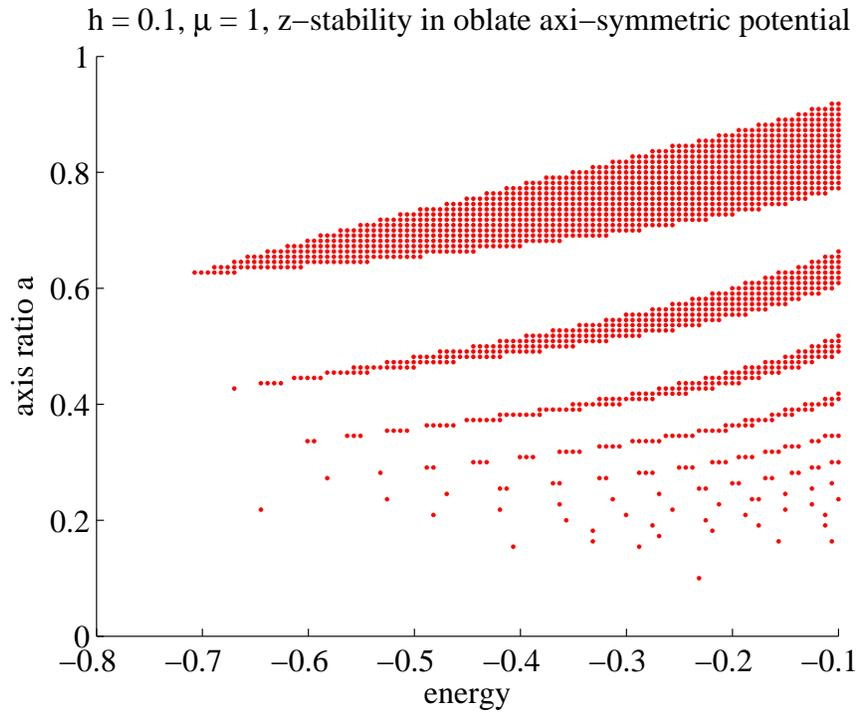


Figure 14: Equatorial stability plot for oblate potential

energy of a Hernquist galaxy with a central black hole, analyzed the rosette-shaped orbits, and then compared them to the orbit as seen from the eccentric frame for various parameter values. Finally we indicated how one might use the eccentric frame to determine stability of planar orbits in axi-symmetric potentials.

References

- Adams, F.C., Bloch, A.M.: Orbits in extended mass distributions: general results and the spirographic approximation. *The Astrophysical Journal*. 629, 204-218 (2005)
- Arnold, V.I.: *Mathematical Aspects of Classical and Celestial Mechanics*. Springer-Verlag (1989)
- Arnold, V.I.: *Dynamical Systems III: Mathematical Aspects of Classical and*

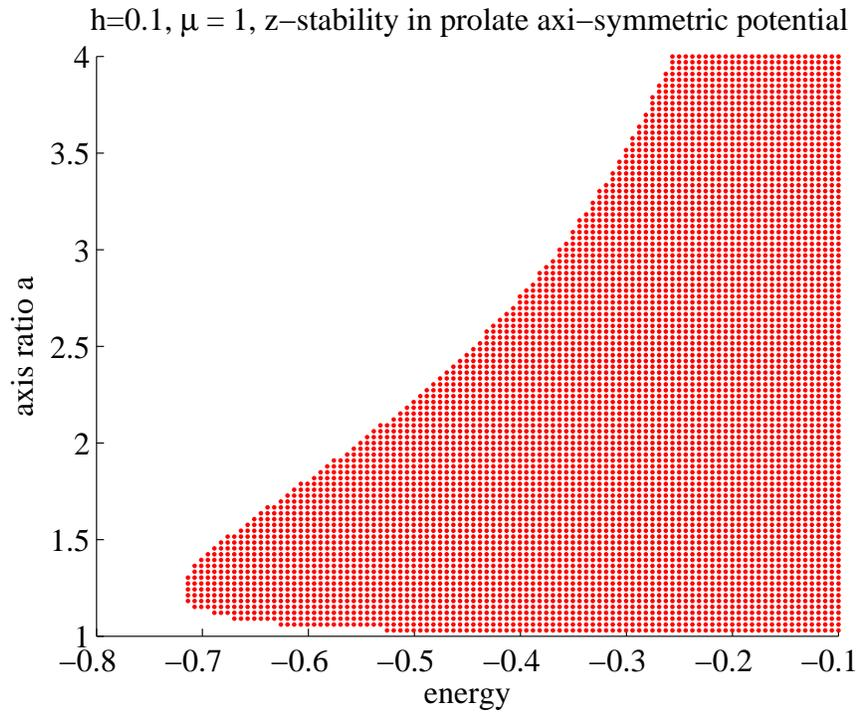


Figure 15: Equatorial stability plot for prolate potential

Celestial Mechanics. Springer-Verlag (1993)
 Brouwer, D., Clemence, G.M.: Methods of Celestial Mechanics. Academic (1961)
 Craig, S., Diacu, F., Lacomba, E. A., Perez, E.: On the Anisotropic Manev Problem. Journal of Mathematical Physics, 40, 1359 - 1375 (1999)
 Diacu, F., Santoprete, M.: Nonintegrability and chaos in the anisotropic Manev problem. Physica D, 156, 39 - 52 (2001)
 Greenwood, D.T.: Classical Dynamics, Dover (1997)
 Hernquist, L.: An analytical model for spherical galaxies and bulges. The Astrophysical Journal. 356, 359-364 (1990)
 Poon, M.Y., Merritt, D.: A self-consistent study of triaxial black hole nuclei. The Astrophysical Journal. 606, 774-787 (2004)
 Roy, A.E.: Orbital Motion. Institute of Physics (1988)
 Whittaker, E.T.: A Treatise on the Analytical Dynamics of Particles and Rigid Bodies. Cambridge University Press (1988)